PHYSICAL REVIEW B VOLUME 27, NUMBER 6 15 MARCH 1983

Electronic structure of semiconductors with doping superlattices

P. Ruden and G. H. Döhler
Max-Planck-Institut für Festkörperforschung, Heisenbergstrasse 1, D-7000 Stuttgart 80, Federal Republic of Germany
(Received 6 August 1982)

The dynamically two-dimensional electronic subband structure and the effective energy gap are tunable quantities in semiconductors with a doping superlattice. We present self-consistent calculations of the electronic states, in the framework of the local-density approximation, as a function of the charge-carrier concentration. A discussion of several superlattices differing in their design parameters exemplifies the wide range of electronic subband structures which may be realized in this type of system.

I. INTRODUCTION

During the last two years a number of experimental investigations have been performed on a new type of artificial semiconductor superlattice consisting of ultrathin *n*- and *p*-type doped layers, which were in some cases separated by undoped (*i*-) intrinsic layers (*n-i-p-i-* crystals).[1–3] The experiments have confirmed the crucial predictions concerning the novel electronic properties of this new class of semiconductors made by one of the present authors (G.H.D.) a long time ago.[4–6] This author had pointed out that doping (or *p-n* junction) superlattices would differ qualitatively not only from homogeneous semiconductors but also from compositional superlattices[7–9] (or heterojunction superlattices) because of the different superlattice potentials. In doping superlattices the conduction and valence bands are modulated by the periodic space-charge potential of the impurities. As a consequence the electron states near the bottom of the conduction band are shifted in their position by half a superlattice period with respect to electron states near the top of the valence bands (*indirect gap in real space*). Compositional superlattices with opposite sign of the conduction- and valence-band—edge discontinuities of the components (type-I superlattices,[7–9]) such as the $Al_xGa_{1-x}As/GaAs$ system, in contrast, exhibit a *direct gap in real space.* Heterojunction superlattices with equal sign for conduction- and valence-band—edge discontinuities between the constituent materials such as the GaSb/InAs system (type-II superlattices[8,9]) also have an indirect gap in real space. The overlap between electron and hole states, however, is still quite large in those systems. Therefore, they do not possess the following basic features of doping superlattices, which result from a very small overlap between electron and hole states.

(1) Owing to extremely long excess-carrier lifetimes, large deviations of the carrier concentrations from the thermal equilibrium values can be induced by rather weak optical excitation or carrier injection from outside.

(2) Because of the spatial separation of electrons and holes the compensating charge of the excess carriers decreases the amplitude of the space-charge—induced superlattice potential and thus increases the effective energy gap drastically. The effective gap of doping superlattices is thus no longer a fixed parameter of the system, but a quantity which may be tuned by changing the nonequilibrium electron and hole concentrations.

The interesting quantum-size effects (quasi-two-dimensional subband formation) which have been the major point of interest in the study of compositional superlattices are present in doping superlattices also. It is evident that the tunability of the (two-dimensional) carrier concentration and of the effective band gap makes the latter kind of superlattice a more fascinating model substance for the study of two-dimensional many-body effects.

In a recent Letter[1] the soundness of the theoretical concept was demonstrated by the observation of a tunable band gap in photoluminescence measurements and of tunable subband separations in Raman scattering experiments. Moreover, excellent quantitative agreement with our self-consistent calculations of the electronic subband structure was found. The first purpose of this paper is to show a more detailed presentation of these calculations including a discussion of many-body effects. Secondly, we will illustrate by a few examples the wide variety of tunable subband structures obtained by different choices of design parameters including the case of a

 ©1983 The American Physical Society

n-i-p-i crystal in which the composition is also modulated periodically (*n-i-p-i* heterojunction superlattice). Finally, we want to provide a basis for our forthcoming discussion of absorption, luminescence, and inelastic light scattering.[10]

II. THEORY OF ELECTRONIC SUBBANDS IN *n-i-p-i* CRYSTALS

A *n-i-p-i* crystal consists of an arbitrary homogeneous semiconductor with a periodic variation of *n*- and *p*-type doping,

$$n_D(z+d)=n_D(z) \quad \text{and} \quad n_A(z+d)=n_A(z)\ , \tag{1}$$

where z is the direction of periodicity and d the superlattice period.

The ground state of the *n-i-p-i* crystal can be described quite easily if there are no other impurities present than the shallow donors and acceptors, if the crystal is "macroscopically compensated," i.e.,

$$\int_{-d/2}^{d/2} n_D(z)dz = \int_{-d/2}^{d/2} n_A(z)dz\ , \tag{2}$$

and if the superlattice period and the doping concentration do not exceed some limiting values to be discussed below. Under these conditions all the impurities will be ionized and the superlattice potential will be the space-charge potential of the impurity distribution,

$$\rho_0(z)=e[n_D(z)-n_A(z)]\ . \tag{3}$$

For the sake of simplicity we will restrict ourselves in the following to the case of homogeneous doping as shown in Fig. 1(a) with rectangular doping profiles which are symmetric with respect to the origin placed in the middle of an *n*-type doped layer.

The space-charge potential of the impurities $v_0(z)$ is obtained by integrating Poisson's equation,

$$\frac{\partial^2 v_0(z)}{\partial z^2}=4\pi e\rho_0(z)/\kappa_0\ , \tag{4}$$

subject to the boundary conditions,

$$\left.\frac{\partial v_0(z)}{\partial z}\right|_{z=0},\quad v_0(0)=0 \tag{5}$$

where κ_0 is the static dielectric constant of the semiconductor. $v_0(z)$ consists of parabolic parts in the doping layers,

$$v_0(z)=\begin{cases}(2\pi e^2 n_D/\kappa_0)z^2 & \text{for } |z|\le d_n/2\\ 2V_0-(2\pi e^2 n_A/\kappa_0)(d/2-|z|)^2 & \text{for } d/2-|z|\le d_p/2\ ,\end{cases} \tag{6}$$

and linear parts in the intrinsic regions,

$$v_0(z)=(2\pi e^2 n_D d_n/\kappa_0)(|z|-d_n/4) \quad \text{for } d_n/2\le|z|\le(d-d_p)/2\ . \tag{7}$$

The maximum height of $v_0(z)$ is $2V_0$, given by

$$2V_0=(2\pi e^2/\kappa_0)(n_D d_n^2/4+n_A d_p^2/4+n_D d_n d_i)\ . \tag{8}$$

For $|z|\ge d/2$, $v_0(z)$ is obtained from a periodic repetition of the expressions (6)–(8).

Figure 1(b) shows the important consequences of the superposition of $v_0(z)$ to the crystal potential. The effective band gap E_g^{eff}, i.e., the difference between the lowest conduction- and the uppermost valence-band states, is lowered by about $2V_0$ compared with the gap of the homogeneous bulk material E_g^0. (Deviations which result from quantum-size effects and from impurity-band formation will be discussed later.) The term *indirect gap in real space* which was used in the Introduction now becomes clear: The lowest conduction-band states are shifted by half a superlattice period with respect to the uppermost valence-band states.

It should be noted that the value of $2V_0$ may exceed the band gap E_g^0 of the unmodulated semiconductor. Such a situation implies the possibility of conduction subbands with energies lower than the upper valence subband edge, which would correspond to a negative effective band gap E_g^{eff}. Actually, under these conditions there will be a finite-electron and -hole concentration in the *n*- and *p*-type layers in the ground state. The compensating space charge of the charge carriers reduces the value of $2V_0$ and changes the shape of the space-charge potential in a self-consistent way to be calculated later. The ground state will then be characterized by electron and hole concentrations $n_0^{(2)}$ and $p_0^{(2)}$ per layer which make the Fermi level equal for both types of carriers (*n-i-p-i* semimetal).

Another case with a finite-carrier concentration in the ground state occurs whenever the *n-i-p-i* crystal is not compensated, i.e., condition (2) does not hold. The ground-state superlattice potential, evidently, has to be calculated self-consistently in such a situation also.

As mentioned in the Introduction, one of the

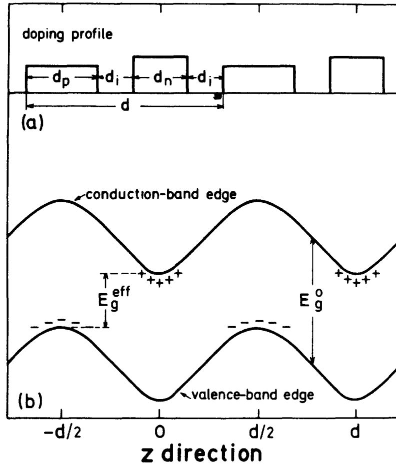

FIG. 1. *n-i-p-i* crystal with constant impurity concentration in the *n*- and *p*-type layers. (a) Periodic doping profile and (b) modulation of conduction- and valence-band edge by the periodic space-charge profile $v_0(z)$ from (6) and (7). Plus signs indicate ionized donor levels near the conduction-band edge and minus signs indicate the negatively charged acceptor levels above the valence-band edge. The effective gap $E_g^{\rm eff}$ is an indirect gap in real space. It differs from the gap of the homogeneous bulk material E_g^0 roughly by $2V_0$ as given by Eq. (8). Corrections to $E_g^{\rm eff}$ due to subband- and impurity-band formation are not shown in this schematic picture.

peculiarities of *n-i-p-i* superlattices is the possibility to induce metastable deviations from thermal equilibrium with different electron and hole quasi-Fermi-levels ϕ_n and ϕ_p, by varying of the electron and hole concentration in the layers. Thus the calculation of the electronic structure of a *n-i-p-i* crystal is not to be restricted to the ground state. The subband energies and wave functions are required as a function of the tunable-carrier concentration.

Before we solve the Schrödinger equation for a *n-i-p-i* crystal we will at least comment on some of the simplifying assumptions which we have made in our calculation of the impurity space-charge potential. So far, and also in the numerical calculations to be discussed, we have treated the space charge of the impurities as homogeneously smeared out in the respective doping regions. In doing so we have neglected the following:

(1) the spatial potential fluctuations which result from the random distribution of impurities in the doped regions and

(2) the point-charge character of the impurities which may lead to bound impurity states or to the formation of impurity bands.

These two points, indeed, limit the possibility to observe quantum-size effects in space-charge—induced potential wells and occasionally were used in the past as an argument against the existence of well-defined quasi-two-dimensional subbands in this kind of system.[11]

Without going into a detailed discussion of this rather complex problem we want to make plausible in the following that in GaAs doping superlattices,

(1) the influence of potential fluctuations is reasonably small,

(2) donor impurity bands may be neglected, and

(3) the formation of acceptor impurity bands must be considered within the typical range of values of design parameters of *n-i-p-i* crystals.

Long-range potential fluctuations are screened by a small concentration of free electrons in the *n*-type layers (holes in the *p*-type layers). Thus they will be unimportant if at least a certain fraction of the impurity space charge per layer is compensated by free carriers. The short-range potential fluctuations result mainly from the random nearest-neighbor impurity distances, which deviate from the mean value r_I (we use the subscripts I to indicate that the following is valid for donors as well as for acceptors). These fluctuations may be estimated by calculating the value of the unscreened Coulomb energy $e^2/\kappa_0 r_I$ of a point charge at distance $r_I=[4\pi/(3n_I)]^{1/3}$. For any reasonable statistical distribution of the impurities the width of the distribution will have roughly the value of the average. The numerical value of $e^2/\kappa_0 r_I$ increases from 15 to 32 meV within the range $5\times10^{17}\ \mathrm{cm}^{-3}\leq n_I\leq 5\times10^{18}\ \mathrm{cm}^{-3}$ with $\kappa_0=12.5$ for GaAs, which is always smaller than the corresponding subband energies. It is clear that the screening by the charge carriers in the layers will actually reduce the potential fluctuation.

The importance of impurity bands may be estimated by the following argument. Let us consider a regular simple cubic array of n_I shallow impurities with ionization energy E_I, Bohr radius a_I, and nearest-neighbor distance $\tilde{r}_I=n_I{}^{-1/3}$. The impurity bandwidth would be approximately $12E_I\exp(-\tilde{r}_I/a_I)$ in a tight-binding picture.

A different approach would be based on the nearly-free-electron model. Here the kinetic energy at the Brillouin-zone boundary becomes

$$\epsilon(\pi/\tilde{r}_I)\approx(\hbar^2/2m^e)\pi^2 n_I^{2/3}\ . \tag{9}$$

A rough estimate of the band splitting is

$$2V(2\pi/\tilde{r}_I)\approx e^2/\kappa_0\tilde{r}_I=e^2 n_I^{1/3}/\kappa_0\ . \tag{10}$$

The tight-binding picture is appropriate for $\tilde{r}_I \gg a_I$ whereas the nearly-free-electron model suits the case $\epsilon(\pi/\tilde{r}_I)\gg 2V(2\pi/\tilde{r}_I)$. With an experimental value for the ionization energy of shallow donors in GaAs $E_D\simeq 6$ meV which corresponds to a Bohr radius, $a_D\simeq 10$ nm, and using $m^e=0.067m_0$ we get

$\epsilon(\pi/\tilde{r}_D) > 2V(2\pi/\tilde{r}_D)$ for $n_D > 10^{16}$ cm^{-3}. Thus even the unscreened impurity potentials act as a relatively small perturbation at donor concentrations which are typical for *n-i-p-i* crystals. Therefore impurity-band formation in the case of the conduction band can be neglected, and it is allowed to replace the actual donor space charge by a homogeneous space charge of density $en_D(z)$ for the calculation of $v_0(z)$ as given in Eqs. (6)–(8).

On the other hand, for the acceptors we find (because of the larger heavy-hole effective mass m^{hh}) a Bohr radius $a_A \simeq 1.8$ nm so that $\tilde{r}_A > a_A$ for $n_A < 10^{20}$ cm^{-3} and $\epsilon(\pi/\tilde{r}_A) > 2V(2\pi/\tilde{r}_A)$ only if $n_A > 2\times 10^{19}$ cm^{-3} using $m^{hh} = 0.6 m_0$. Thus we can expect an impurity band in the *p*-type layers of a *n-i-p-i* structure unless n_A is extremely high. This result does not signify that hole subbands do not exist in the *p*-type layers or that they are unimportant. The presence of an acceptor impurity band implies, however, important consequences for the calculation of the self-consistent potential. The population of the acceptor impurity band by holes is equivalent to a neutralization of the negatively charged acceptors. It is, therefore, a reasonably good approximation to consider the central part of width $d_p^0 = p^{(2)}/n_A$ in the *p*-type layers as neutral, if $p^{(2)}$ holes per layer are present in the sample.

We will now proceed by discussing the electronic subband structure in the *n*-type layers in the framework of the local-density-functional formalism of Hohenberg and Kohn[12] and Kohn and Sham.[3] Together with the effective-mass approximation[14] this formalism leads to a Schrödinger-type equation of the form

$$[-(\hbar^2/2m^e)\nabla^2 + v_0(z) + v_H(z) + v_{xc}(z)]\psi_{\mu\vec{k}}(\vec{r}) = \epsilon_{\mu\vec{k}}\psi_{\mu\vec{k}}(\vec{r}) . \quad (11)$$

Since the potential does not depend on x or y and is periodic in z with the periodicity d we can write for the wave functions

$$\psi_{\mu\vec{k}}(\vec{r}) = (1/\sqrt{A})\exp(i\vec{k}_{\|}\cdot\vec{r}_{\|})\xi_{\mu k_z}(z) , \quad (12)$$

where $\vec{k}_{\|}$ is a wave vector parallel to the doping layers. A is the normalization area and $\zeta_{\mu k_z}(z)$ is the superlattice Bloch function of subband μ and wave vector k_z $(-\pi/d \le k_z < \pi/d)$, with the lattice periodic part $u_{\vec{k}=0}(\vec{r})$ neglected. For the eigenvalues $\epsilon_{\mu\vec{k}}$ we thus get

$$\epsilon_{\mu\vec{k}} = \epsilon_{\mu k_z} + (\hbar^2 k_{\|}^2/2m^e) , \quad (13)$$

and the Bloch functions $\zeta_{\mu k_z}(z)$ and the eigenvalues $\epsilon_{\mu k_z}$ are to be determined self-consistently from

$$\left[-\left[\frac{\hbar^2}{2m^e}\right]\left[\frac{\partial^2}{\partial z^2}\right] + v_0(z) + v_H(z) + v_{xc}(z)\right]\xi_{\mu k_z}(z) = \epsilon_{\mu k_z}\xi_{\mu k_z}(z) . \quad (14)$$

The Hartree contribution of the electrons to the self-consistent potential is given by the solution of Poisson's equation

$$\frac{\partial^2 v_H(z)}{\partial z^2} = -\frac{4\pi e^2 n(z)}{\kappa_0} , \quad (15)$$

subject to the boundary conditions

$$\left.\frac{\partial v_H(z)}{\partial z}\right|_{z=0} = 0, \quad v_H(0) = 0 \quad (16)$$

with the electron density

$$n(z) = 2\sum_{\mu\vec{k}} |\xi_{\mu k_z}(z)|^2 \times \Theta(\phi_\mu - \epsilon_{\mu k_z} - (\hbar^2 k_{\|}^2/2m^e) - E_c) . \quad (17)$$

E_c is the energy of the bottom of the conduction band at $z=0$.

The local exchange and correlation potential is obtained from

$$v_{xc}(z) = \epsilon_{xc}(n(z)) + n(z)(\delta\epsilon_{xc}/\delta n) , \quad (18)$$

where $\epsilon_{xc}(n)$ is the exchange and correlation energy per electron of a homogeneous electron gas of the (local) density n. Since the electronic densities of interest in *n-i-p-i* crystals are usually very high, i.e., the mean distance between two electrons is short compared to the effective-mass Bohr radius $a_D^{EMA} = a_B\kappa_0(m_0/m^e)$, we will take

$$-\epsilon_{xc} = -\epsilon_x = (0.916/r_s)(e^2/2\kappa_0 a_D^{EMA}) \quad (19)$$

with

$$r_s = [4\pi/(3n)]^{1/3}/a_D^{EMA} . \quad (20)$$

The inclusion of higher-order correlation terms does not affect the results appreciably. The contribution of the holes in the *p*-type layers to the self-consistent potential is not written explicitly since it can be incorporated into $v_0(z)$, as discussed above.

In most cases of interest only the lowest electronic subbands are partially occupied. For these low subbands and typical doping parameters an extreme tight-binding approach is correct, i.e., the subbands are flat in the k_z direction. The Bloch function can be written as

$$\xi_{\mu k_z}(z)=(1/\sqrt{N_{\rm SL}})\sum_m \exp(ik_z m_d)\Phi_\mu(z-md)\ , \tag{21}$$

where $N_{\rm SL}$ is the number of superlattice periods in the crystal and $\Phi_\mu(z-md)$ is the wave function of subband μ centered at the n-type layer with label m. Obviously, the square modulus of $\xi_{\mu k_z}(z)$ is in this case independent of k_z, and the electron density may be written as

$$n(z)=\sum_\mu n_\mu^{(2)}\,|\,\xi_{\mu 0}(z)\,|^2 N_{\rm SL} \tag{22}$$

$$=\sum_{\mu,m} n_\mu^{(2)}\,|\,\Phi_\mu(z-md)\,|^2\ , \tag{23}$$

where the population $n_\mu^{(2)}$ of the μth subband is determined by the requirement of equal Fermi levels in occupied subbands,[15]

$$\epsilon_\mu+(\hbar^2/2m^e)2\pi n_\mu^{(2)}=\epsilon_0+(\hbar^2/2m^e)2\pi n_0^{(2)} \tag{24}$$

with

$$\sum_{\mu_{\rm occ}} n_\mu^{(2)}=n^{(2)}\ . \tag{25}$$

We have solved Eq. (14) self-consistently by direct numerical integration at $k_z=0$ and $k_z=\pi/d$. The boundary conditions to be imposed are as follows: for $\mu=0,2,4,\ldots$,

$$\left.\frac{\partial\xi_{\mu 0}(z)}{\partial z}\right|_{z=0}=\left.\frac{\partial\xi_{\mu,\pi/d}(z)}{\partial z}\right|_{z=0}=0\ , \tag{26}$$

$$\left.\frac{\partial\xi_{\mu 0}(z)}{\partial z}\right|_{z=d/2}=0,\quad \xi_{\mu,\pi/d}(d/2)=0\ , \tag{27}$$

and for $\mu=1,3,5,\ldots$,

$$\xi_{\mu 0}(0)=\xi_{\mu,\pi/d}(0)=0\ , \tag{28}$$

$$\xi_{\mu 0}(d/2)=0,\quad \left.\frac{\partial\xi_{\mu,\pi/d}(z)}{\partial z}\right|_{z=0}=0\ . \tag{29}$$

Some *n-i-p-i* crystal subbands with a finite k_z dispersion may become occupied in the very highly excited state. It is then usually sufficient to calculate the potential once with the wave functions associated with $k_z=0$ and once with those at $k_z=\pi/d$ and then to average.

III. RESULTS AND DISCUSSION

We have solved the system of Eqs. (14)–(25) self-consistently, taking into account the boundary conditions (26)–(29) and averaging over occupied bands, if necessary as mentioned above, for different *n-i-p-i* crystals, including *n-i-p-i* heterojunction superlattices. To illustrate the variety of electronic structures obtainable with different design parameters of the system we present results for a structure without intrinsic layers (Figs. 2–4), for an extreme *n-i-p-i* structure with thin doping layers and rather wide intrinsic layers (Figs. 5–7) and, finally, for a *n-i-p-i* heterojunction superlattice composed of a periodic *n-p*-type doping structure with undoped layers of a smaller band-gap material interspersed in the middle of the *n*-type layers (Figs. 8 and 9). To facilitate the comparison of these systems we have kept one parameter fixed, namely, the superlattice constant d. We would like to emphasize the dependence of the subband structure on the shape of the doping profiles.

As the first structure we have chosen the sample for which we have compared quantitative results with experiments in Ref. 1. It is composed of 40-nm-thick GaAs layers with constant doping concentrations $n_D=n_A=10^{18}$ cm^{-3} and does not contain intrinsic layers. In Fig. 2 the solid lines represent the energies for the bottom of the various subbands referred to the position of the hole quasi-Fermi-level ϕ_p as a function of the two-dimensional carrier concentration per layer. We have assumed that ϕ_p coincides with the acceptor level in the central part of the p-type layers (acceptor ionization energy $E_A=28$ meV for Be acceptors).

It should be noted that the curve $\phi_n-\phi_p$ vs $n^{(2)}$ (dashed-dotted line) does not deviate appreciably from a parabola with a vertex at $n^{(2)}=n_D d_n=4\times10^{12}$ cm^{-2}. This behavior reflects the parabolic relation between injected carriers and the quasi-Fermi-level distance $\phi_n-\phi_p$ which would be obtained from a simple classical treatment of the problem.

At $n^{(2)}=0$ all the subbands shown are nearly equally spaced with

$$\epsilon_\mu-\epsilon_{\mu-1}=\hbar[4\pi e^2 n_D/(\kappa_0 m^e)]^{1/2}$$

since the bare potential $v_0(z)$ deviates appreciably from a harmonic potential only at higher energies. With increasing carrier concentration the subband distances decrease monotonously as the shape of the self-consistent potential

$$v_{\rm sc}(z)=v_0(z)+v_H(z)+v_{\rm xc}(z) \tag{30}$$

flattens and broadens due to screening of the fixed-impurity space charge (see Fig. 3). In order to show the behavior of the subbands, in particular the finite width of the upper bands at large carrier concentrations, the subband energies are displayed more clearly once more in Fig. 2 as an inset on an expanded energy scale and with the maximum of $v_{\rm sc}(z)$, i.e.,

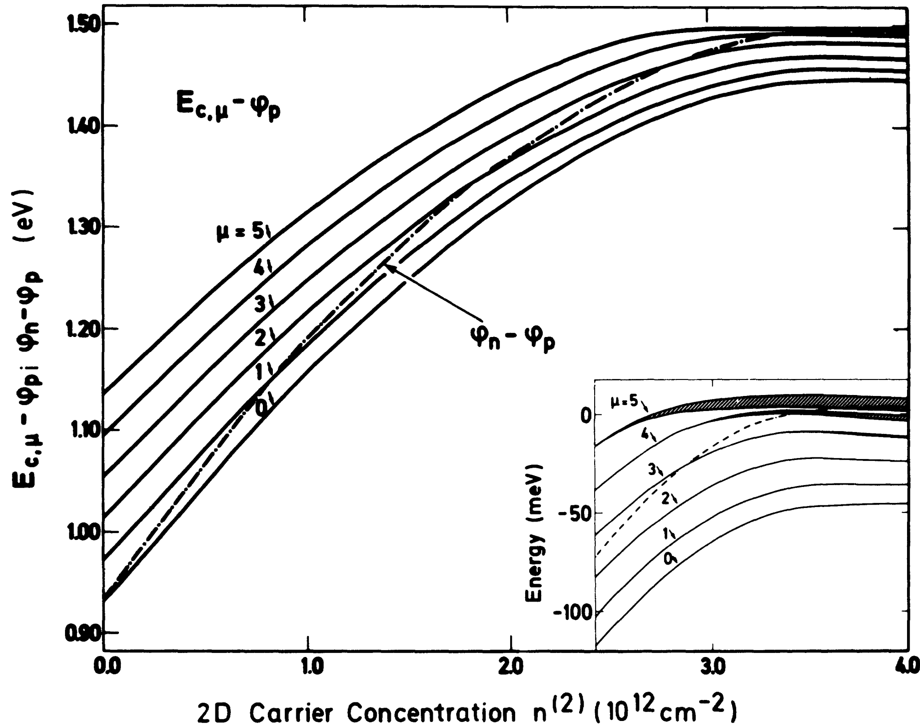

FIG. 2. Subband energies and a quasi-Fermi-level as a function of the electron concentration per period $n^{(2)}$ for a doping superlattice with constant doping $n_D=n_A=1\times10^{18}$ cm^{-3} in the n- and p-type layers, respectively, and with $d_n=d_p=40$ nm and $d_i=0$. $E_{c,\mu}=E_c+\epsilon_\mu$, the bottom of the μth conduction subband, and ϕ_n, the electron quasi-Fermi-level, are referred to the position of the hole quasi-Fermi-level ϕ_p in the acceptor impurity band. The inset shows the same subbands for large values on $n^{(2)}$ on an expanded energy scale and with the maximum of the self-consistent potential chosen as zero. The finite subband width due to the k_z dispersion becomes appreciable near zero energy, which corresponds to the classical free-particle threshold energy.

the classical free-particle threshold as the zero of energies. The band*width* becomes appreciable only when the energies nearly reach this threshold. For energies above the threshold, however, the subband *gap* becomes rather narrow. Thus the subbands

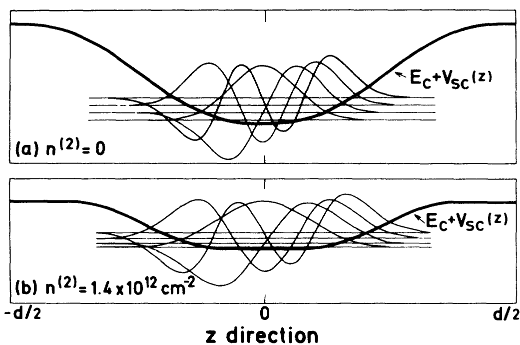

FIG. 3. Self-consistent potential $v_{sc}(z)$ (thick solid line), conduction-subband energies, and envelope wave functions for one period of a superlattice with the same design parameters as in Fig. 2. (a) Ground state ($n^{(2)}=0$) and (b) excited state ($n^{(2)}=1.4\times10^{12}$ cm^{-2}).

change their character from tight-binding to nearly-free-electron behavior within a few meV. This is to be expected because of the wide barrier between neighboring quantum wells. Another detail which should be noted is the position of ϕ_n at $n^{(2)}=4\times10^{12}$ cm^{-2} (which corresponds classically to a neutralization of all donors and acceptors by electrons and holes, respectively), which is found to be only slightly above the threshold energy. This means that the electrons almost exactly fill up to the top the self-consistent potential well formed by the impurity charges and the free carriers together.

Figure 4 demonstrates the influence of $v_{xc}(z)$ on the subband splitting. For $n^{(2)}>10^{11}$ cm^{-2} the difference between the results with $v_{xc}(z)$ taken into account (solid lines) and the Hartree energies (dotted lines) remains nearly constant and relatively small compared to exchange and correlation corrections in Si metal-oxide-semiconductor structures. The nearly constant exchange and correlation contribution is a consequence of the fact that the electron distribution $n(z)$ only widens with increasing $n^{(2)}$ but does not appreciably increase in height which is close to

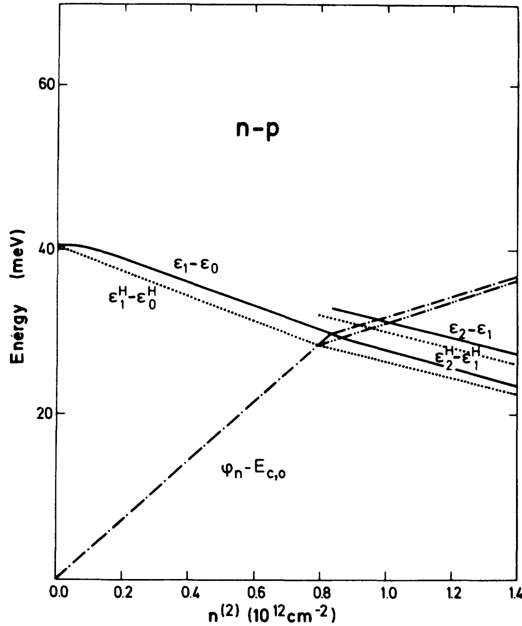

FIG. 4. Comparison of the subband splitting between occupied and the nearest-neighbor subbands for low carrier concentrations calculated with (solid lines) and without (dotted lines) exchange and correlation corrections. The dashed-dotted and dashed-double-dotted lines represent the Fermi energy of the lowest subband $\phi_n - E_{c,0}$ for the case with and without exchange and correlation corrections. The design parameters are those of Fig. 2.

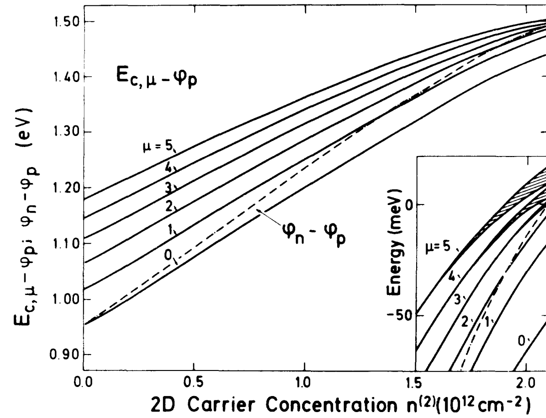

FIG. 5. Subband energies and a quasi-Fermi-level as a function of the electron concentration per period $n^{(2)}$ for a n-i-p-i superlattice with the design parameters $n_D = n_A = 5.25\times 10^{18}$ cm^{-3} and $d_n = d_p = 4$ nm, $d_i = 36$ nm. $E_{c,\mu} = E_c + \epsilon_\mu$, the bottom of the μth conduction subband, and ϕ_n, the electron quasi-Fermi-level, are referred to the position of the hole quasi-Fermi-level ϕ_p in the acceptor impurity band. The inset shows the same subbands for large values of $n^{(2)}$ on an expanded energy scale and with the maximum of the self-consistent potential chosen as zero. The finite subband width due to the k_z dispersion becomes appreciable near zero energy which corresponds to the classical free-particle energy.

n_D over a layer of the width $n^{(2)}/n_D$.

The corresponding results for a n-i-p-i structure with very thin doping layers of only 4 nm and a thickness of 36 nm for the intrinsic layers are given in Figs. 5–7. The doping concentration $n_D = n_A = 5.25\times 10^{18}$ cm^{-3} has been chosen such that the effective gap has approximately the same value for $n^{(2)}=0$ as in the former case. From Fig. 5 we see that the subband distances are now larger at small μ values and that they decrease at higher μ since the bare potential $v_0(z)$ has a triangular rather than a parabolic shape. The relation between $\phi_n - \phi_p$ and $n^{(2)}$ is quite close to a linear dependence because of the wide nearly constant field zones in the intrinsic layers. The subband spacing also decreases with increasing $n^{(2)}$. In contrast to the former case, however, the relative decrease is weaker and affects the higher subbands more than the lower ones: $\epsilon_1 - \epsilon_0$ decreases only by 1/1.8 between $n^{(2)}=0$ and $n^{(2)} = n_D d_n$ compared to 1/4.3 in the former case. $\epsilon_2 - \epsilon_1$, however, decreases now faster than $\epsilon_1 - \epsilon_0$, namely by 1/4.2, whereas the corresponding decrease of $\epsilon_2 - \epsilon_1$ by 1/3.5 was less pronounced for the first example. The two cases exemplify that it is possible to tailor details of the subband structure and of the relation between $\phi_n - \phi_p$ and $n^{(2)}$ simply by an appropriate choice of the design parameters n_D, n_A, d_n, d_p, and d_i, or by even going one step further and changing from zones of constant doping to continuous doping profiles $n_D(z)$ and $n_A(z)$.

The variation of the bandwidth near the classical free-particle threshold energy is less abrupt for the

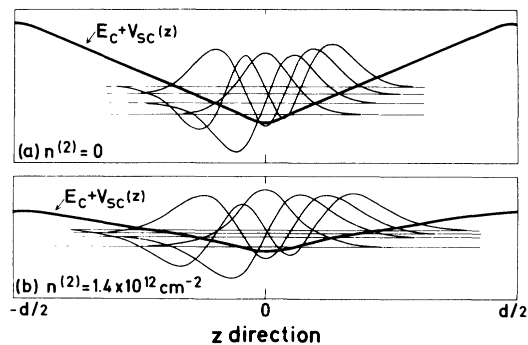

FIG. 6. Self-consistent potential $v_{sc}(z)$ (thick solid line), conduction-subband energies, and envelope wave functions for one period of a superlattice with the same design parameters as in Fig. 5. (a) Ground state ($n^{(2)}=0$) and (b) excited state ($n^{(2)} = 1\times 410^{12}$ cm^{-2}).

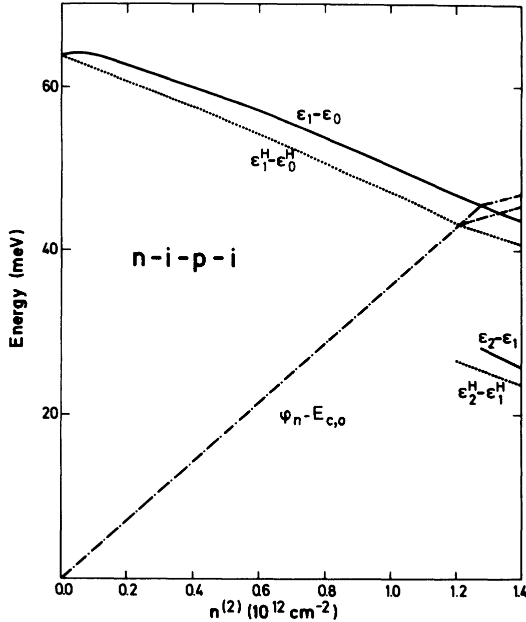

FIG. 7. Comparison of the subband splitting between occupied and nearest-neighbor subbands for low carrier concentrations calculated with (solid lines) and without (dotted lines) exchange and correlation corrections. The dashed-dotted and dashed-double-dotted lines represent the Fermi energy of the lowest subband $\phi_n - E_{c,0}$ for the case with and without exchange and correlation correction. The design parameters are those of Fig. 5.

n-i-p-i case with wide intrinsic layers than for the first example (compare the corresponding insets in Figs. 2 and 5), due to the smaller width of the zone with maximum barrier height (see Figs. 6 and 3 for a comparison).

Finally, a comparison of the exchange and correlation shift as depicted in Fig. 7 for the genuine *n-i-p-i* sample with the corresponding results for the sample without intrinsic layers shows that not only the absolute value of the $\epsilon_1 - \epsilon_0$ subband spacing is increased but even the relative importance of the exchange and correlation correction is larger. The result becomes plausible if we consider that in the present case the lowest subband wave function is less extended in the z direction for a given carrier concentration $n^{(2)}$. The resulting larger local density lowers the self-consistent potential in this region. Therefore the energy of the ϵ_0 band is lowered considerably, whereas the much more extended ϵ_1 band is much less affected by the exchange and correlation correction.

Our last example is a *n-i-p-i* heterojunction crystal consisting of *n*- and *p*-type doped layers of $Al_{0.2}Ga_{0.8}As$ with a layer thickness of $d_n = 20$ nm, $d_p = 40$ nm, and doping concentrations $n_D = 2 \times 10^{18}$

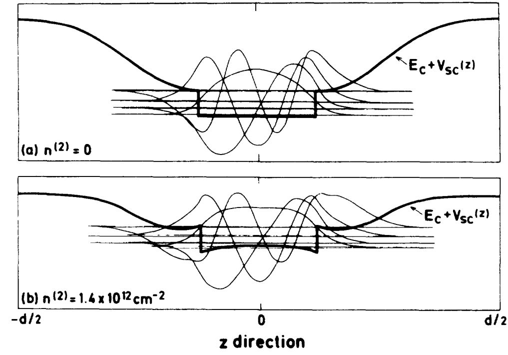

FIG. 8. Self-consistent potential $v_{sc}(z)$ (thick solid line), conduction-subband energies, and envelope wave functions for one period of an $Al_{0.2}Ga_{0.8}As$/GaAs *n-p* heterojunction superlattice with the design parameters $n_D = 2 \times 10^{18}$ cm^{-3}, $n_A = 10^8$, cm^{-3}, $d_n = 20$ nm, $d_p = 40$ nm, $d_i = 0$, $d_{GaAs} = 20$ nm. (a) Ground state ($n^{(2)} = 0$) and (b) excited state ($n^{(2)} = 1.4 \times 10^{12}$ cm^{-2}). The discontinuity in the potential reflects the transition from *n*-type doped $Al_{0.2}Ga_{0.8}As$ to undoped GaAs. The *p*-type layers do not contain GaAs layers in this example.

cm^{-3}, $n_A = 1 \times 10^{18}$ cm^{-3}. The *n*-type layers are separated into two layers (of thickness $d_n/2$) by an intrinsic GaAs layer of thickness $d_{GaAs} = 20$ nm.

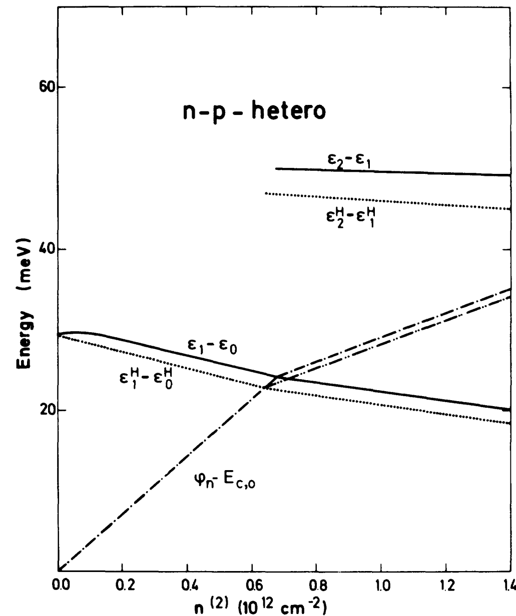

FIG. 9. Comparison of subband splitting between occupied and nearest-neighbor subbands for low carrier concentrations calculated with (solid lines) and without (dotted lines) exchange and correlation corrections. The dashed-dotted and dashed-double-dotted lines represent the Fermi energy of the lowest conduction subband $\phi_n - E_{c,0}$ for the case with and without the exchange and correlation correction. The design parameters are those of Fig. 8.

This system thus provides an example of a semiconductor superlattice whose subband structure in the ground state is determined by the doping parameters, the width of the GaAs layer, and the Al content of the $Al_xGa_{1-x}As$ alloy. Through its dependence on the variable carrier concentration $n^{(2)}$ the subband structure may be tuned over a wide range as in normal *n-i-p-i* crystals. This is not the case in the modulation doped heterojunction superlattices (the dependence of the subband structure on the electron concentration shown in Fig. 5 of Ref. 14 corresponds to a variation of the doping parameters and not to change in a tunable charge carrier concentration). The dependence of $E_{c,\mu}-\phi_p$ on $n^{(2)}$ is quite similar to the results of the first example and is, therefore, not shown here. It is interesting to consider the subband spacing as a function of $n^{(2)}$ because of the different nature of the quantum wells (Fig. 9). The spatial extent of the wave functions is now determined by the width of the GaAs layer (Fig. 8), whereas in the case of the space-charge–induced quantum wells it varied from one subband to another and changed appreciably as a function of $n^{(2)}$. Consequently, the subband energies are less dependent on the carrier concentration in a *n-i-p-i* heterojunction crystal. A remarkable result is the relatively large difference in the exchange and correlation corrections for the $\epsilon_1-\epsilon_0$ and the $\epsilon_2-\epsilon_0$ subband separations.

IV. CONCLUSIONS

We have shown that the subband structure and the effective band gap in *n-i-p-i* crystals can be tuned by variation of the nonequilibrium carrier concentration. Our discussion was exemplified by three systems with very different design parameters to show how the subband structure and its dependence on $n^{(2)}$ can be tailored within wide limits. The *n-i-p-i* heterojunction superlattice, in particular, may become of interest in the future because of the high electron mobility in the GaAs layers and the weak broadening of the subbands due to statistical potential fluctuations. These features will be more pronounced when the GaAs layers are separated from the doped $Al_xGa_{1-x}As$ layers by an intrinsic $Al_xGa_{1-x}As$ space layer as is the practice in normal modulation doped multiple–quantum-well structures.[16]

We have not discussed the hole subbands. Their calculation is quite straightforward as the self-consistency problem is a trivial one if the holes populate the acceptor impurity band. The only problem would be the coupling between light- and heavy-hole states due to the space-charge potential. The solution of this problem may, however, be of academic interest only, since the subband structure of the heavy holes may be broadened too much by random potential fluctuations in order to be detectable. In a planned subsequent paper we will, however, provide examples showing that the light-hole subbands will be relevant for the observation of a steplike structure in the optical-absorption coefficient.

We have restricted our discussion to semiconductors with a band structure of the GaAs type. Obviously, some of our results would change dramatically if, e.g., a many-valley band structure of the host material were considered.

[1]G. H. Döhler, H. Künzel, D. Olego, K. Ploog, P. Ruden, H. J. Stolz, and G. Abstreiter, Phys. Rev. Lett. 47, 864 (1981).

[2]G. H. Döhler, H. Künzel, and K. Ploog, Phys. Rev. B 25, 2616 (1982).

[3]H. Künzel, G. H. Döhler, A. Fischer, and K. Ploog, Appl. Phys. Lett. 38, 171 (1981).

[4]G. H. Döhler, Phys. Status Solidi B 52, 79 (1972).

[5]G. H. Döhler, J. Vac. Sci. Technol. 16, (3),851 (1979).

[6]G. H. Döhler and K. Ploog, Prog. Cryst. Growth Charact. 2, 145 (1979).

[7]L. Esaki and R. Tsu, IBM J. Res. Dev. 14, 61 (1970).

[8]G. A. Sai-Halasz, in *Proceedings of the 14th International Conference on the Physics of Semiconductors, Edinburgh, 1978,* edited by B. L. H. Wilson (IOP, Bristol, 1978).

[9]T. Ando, A. Fowler, and F. Stern, Rev. Mod. Phys. 54, 2 (1982), and references therein.

[10]P. Ruden and G. H. Döhler, Phys. Rev. B 27, 3547 (1983).

[11]Comments made by several colleagues in previous discussions with one of the authors (G.H.D.).

[12]P. Hohenberg and W. Kohn, Phys. Rev. 136, B864 (1964).

[13]W. Kohn and L. Sham, Phys. Rev. 140, A1133 (1965).

[14]Subband-structure calculations using this type of approach have, e.g., been carried out for $Al_xGa_{1-x}As$/GaAs superlattices by T. Ando and S. Mori, J. Phys. Soc. Jpn. 47, 1518 (1979).

[15]G. H. Döhler, Surf. Sci. 73, 97 (1978).

[16]H. L. Störmer, A. Pinczuk, A. C. Gossard, and W. Wiegmann, Appl. Phys. Lett. 38, 681 (1981).